Thermal Radiation towards the Sideledge in Alumina Reduction Cells

Asbjørn Solheim[1], Henrik Gudbrandsen[2]
Nils-Håvard Giskeødegård [3], Steinar Kolås [3], Eirik Manger [3] and Nancy J. Holt [4]
1. Chief Scientist
2. Research Engineer
SINTEF Materials and Chemistry, Trondheim, Norway
3. Principal Engineer
4. Manager External R&D (nancy.jorunn.holt@hydro.com)
Hydro Aluminium AS, Primary Metal Technology, Øvre Årdal, Norway
Corresponding author: asbjorn.solheim@sintef.no

Abstract

When performing energy balance calculations for aluminium electrolysis cells, it is often found that the computed superheat is higher than the measured superheat. The deviation can be explained by thermal radiation between the interior of the cell and the sideledge, effectively increasing the heat transfer coefficient. As it appeared that radiation through molten fluorides has never been directly observed, an apparatus was designed for detecting temperature variations when thermocouples were exposed to or shielded against radiation from a heating element placed in a crucible containing industrial bath. CFD calculations indicated that the recorded temperature would be little influenced by changes in the convection pattern upon shifting the radiation shield, while a temperature response in the order of 1 °C due to radiation could be expected. The estimates were confirmed by experiments. The recorded temperature responses were in the range between 0.5 °C and 2.5 °C depending on the power in the heating element. The results strongly indicate that radiation through the bath indeed takes place, but neither calculations nor experiment are accurate enough to allow for determination of emissivities or attenuation coefficients. The effect on the heat transfer coefficient may be up to 400 $Wm^{-2}K^{-1}$.

Key words: Heat transfer in aluminium electrolysis cell; radiation from bath to sideledge; heat transfer coefficient from bath to sideledge.

1. Introduction

There have been a number of studies concerning heat transfer between bath and sideledge in aluminium reduction cells. Today, it is fairly well established that the convective heat transfer coefficient (h) is 700 - 1000 $Wm^{-2}K^{-1}$ [1 - 4]. The heat transfer coefficient, the heat flux between the bath and the ledge (q), and the superheat (ΔT, difference between the bath temperature and the liquidus temperature) are related by the well-known equation

$$q = h\Delta T \quad (1)$$

The superheat is measured routinely in most aluminium companies. The heat flow can be found by measurement as well as by modelling. By calculating "backwards" from a given heat flow, it often turns out that the measured superheat is lower than the computed superheat. There is no specific reason to believe that there are systematic errors in the superheat detection, which indicates that the heat transfer coefficient must be higher than what was used in the superheat computation [5].

A possible explanation for this "superheat enigma" would be that the heat transfer coefficient is influenced by thermal radiation between the sideledge and the interior of the cell, which was

earlier suggested by Gan and Thonstad [2]. On this background, it was decided to design a simple experiment for detection of radiation through molten cryolitic bath. The experimental details and the results obtained are reported in the present paper.

2. Theory

2.1. Radiation Intensity and Transparency

Infrared radiation can be defined as electromagnetic waves with wavelengths above 700 nm. The intensity of radiation from a black body is governed by Planck's law, which relates the intensity of radiation and the wavelength (or frequency) at different temperatures. A graphical representation of Planck's law is shown in Figure 1. The maximum intensity at 1000 ºC is at about 2000 nm.

Radiation between two surfaces can take place only if the intermediate medium is transparent to radiation within the actual range of wavelengths. Some data concerning the transparency range for solid compounds relevant for the aluminium electrolysis are shown in Table 1. As can be observed, most of the compounds are transparent in the entire range of wavelengths shown in Figure 1. There is no specific reason to believe that the transparency disappears upon melting; *e.g.*, it is well known that molten cryolite is "as clear as water". Therefore, the data in Table 1 strongly indicate that industrial bath will be transparent to heat radiation.

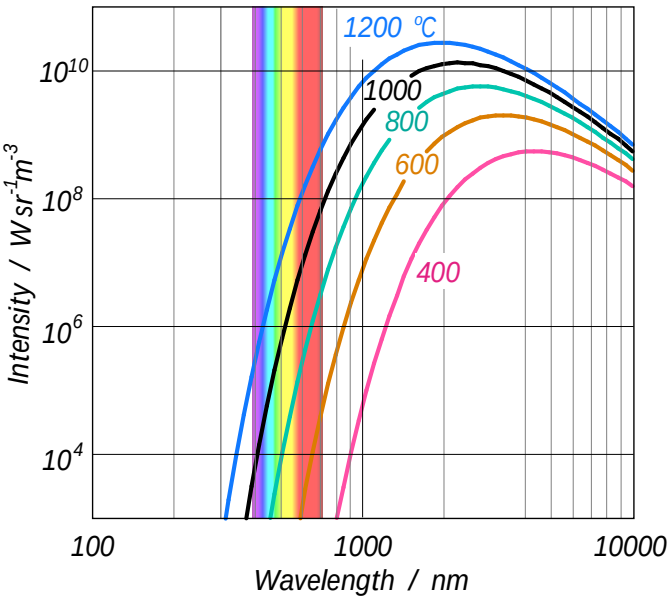

Figure 1. Radiation intensity as a function of the wavelength. Visible light is in the range of 390 - 700 nm.

Table 1. Transparency range for some relevant solid compounds. Data taken from Merck [6].

Compound	Formula	Transparency range
Alumina	Al_2O_3	200 - 5 000 nm
Aluminium fluoride	AlF_3	150 - 10 000 nm
Chiolite	$Na_5Al_3F_{14}$	200 - 14 000 nm
Cryolite	Na_3AlF_6	200 - 14 000 nm
Magnesium fluoride	MgF_2	150 - 7 000 nm

2.2. Radiation Between Surfaces

The theory concerning electromagnetic radiation can be found in many textbooks, *e.g.*, Transport Phenomena [7]. An exact calculation concerning electromagnetic radiation tends to be complex, as it requires knowledge about view angles calculated from the geometry, as well as emissivities and temperatures for all surfaces involved. The general equation for radiation between two surfaces 1 and 2 is [8]:

$$Q_{12} = \frac{\sigma \cdot \left[T_1^4 - T_2^4\right]}{\frac{1}{A_1 F_{12}} + \frac{1}{A_1}\left(\frac{1}{\varepsilon_1} - 1\right) + \frac{1}{A_2}\left(\frac{1}{\varepsilon_2} - 1\right)} \quad [\mathrm{W}] \qquad (2)$$

Where: σ Stefan-Bolzmann constant (5.67×10^{-8} $\mathrm{Wm^{-2}K^{-4}}$),
T Absolute temperature, K
A Surface area, $\mathrm{m^2}$
F_{12} View factor between the surfaces and
ε Emissivity, number.

For two parallel surfaces without edge effects ($A_1 = A_2$ and $F_{12} = 1$), the equation reduces to

$$q_{12} = \frac{\sigma \cdot \left[T_1^4 - T_2^4\right]}{1/\varepsilon_1 + 1/\varepsilon_2 - 1} \quad [\mathrm{Wm^{-2}}] \qquad (3)$$

and if the emissivities are equal

$$q_{12} = \frac{\varepsilon\, \sigma \cdot \left[T_1^4 - T_2^4\right]}{2 - \varepsilon} \quad [\mathrm{Wm^{-2}}] \qquad (4)$$

2.3. Heat Transfer Coefficient

In the case of two parallel surfaces without end effects and with equal emissivities, the apparent heat transfer coefficient due to radiation (h_{rad}) can be defined as

$$h_{rad} = \frac{q_{12}}{T_1 - T_2} = \frac{\varepsilon\, \sigma \cdot \left[T_1^4 - T_2^4\right]}{(2 - \varepsilon) \cdot (T_1 - T_2)} \quad [\mathrm{Wm^{-2}K^{-1}}] \qquad (5)$$

If the temperature difference between the surfaces is small, Equation (5) can be factorized, using $(T_1+T_2) \approx 2T_{av}$ where the latter is the average temperature,

$$h_{rad} \approx \frac{4\varepsilon\, \sigma T_{av}^3}{2 - \varepsilon} \qquad (6)$$

A graphical representation of Equation (6) is shown in Figure 2. The radiation term and the convective heat transfer coefficient (h_{conv}) are additive:

$$h = h_{conv} + h_{rad} \qquad (7)$$

It follows from Figure 2 that if the emissivity is high and the bath is transparent to radiation, the effect on the heat transfer coefficient will be considerable. The emissivities of solid materials except non-oxidized metals tend to be about 0.9.

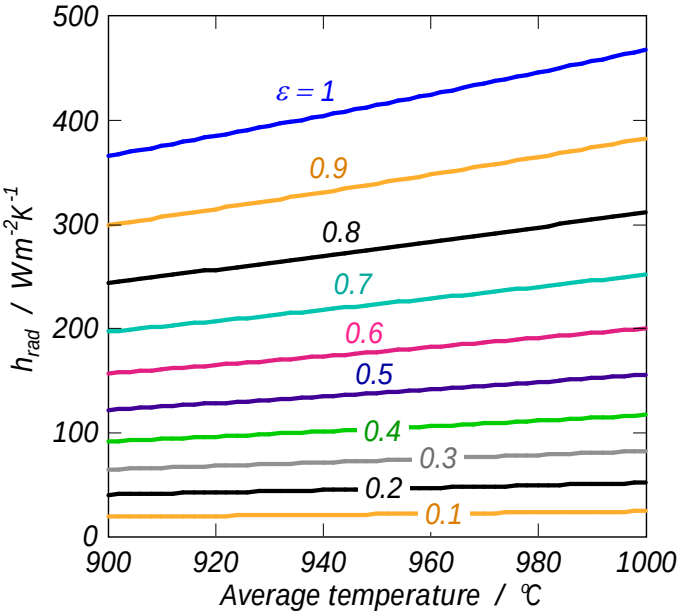

Figure 2. Heat transfer coefficient due to radiation as a function of the average temperature at different emissivity.

3. Experimental

3.1. Basic Idea and Experimental Set-up

The basic idea was to use thermocouples for detecting radiation from a heating element placed in a cryolitic melt. It was decided to locate the heating element at the centre of a graphite crucible and surround it by thermocouples (TC) and a revolving radiation shield, as shown in Figure 3. A picture of the equipment during assembly is placed in Figure 4.

In Figure 3, TC 1 is exposed to radiation, while TC 3 is shielded. By rotating the shield by 180 degrees, TC 3 will be exposed while TC 1 becomes shielded. The radiation shields were made of 4 sheets of 0.5 mm stainless steel, welded to a flange at the end of the steel rod used for carrying the 20 mm diameter heating element. The TC sheaths were 12 mm in diameter and contained Pt-Pt10Rh TCs protected by 3 mm diameter 2-bore sintercorundum tubes. The heating element was made of 0.5 mm Pt wire wound around a 5 mm diameter sintercorundum tube. The element was supplied with separate wires for current supply and for measuring the voltage drop along the active part of the element.

3.2. Estimates of Temperature Response

It had to be verified that the basic idea could be used for detection of radiation, and the experimental design described above was partly based on modelling. The modelling work comprised estimates of the necessary power in the heating element, the effectiveness of the radiation shield, the temperature response in the TCs (provided that the melt is completely transparent to radiation), the effect of natural convection, and the time constant for the TC response. No end or edge effects were taken into account, and the accuracy of the calculation

was not expected to be better than within a factor of 2. For the estimate of radiation, Equation (2) was applied, assuming emissivities of 1 for all surfaces:

$$Q_{12} = \sigma \left[T_1^4 - T_2^4 \right] A_1 F_{12} \qquad (8)$$

The view factors were taken from a collection of equations for different geometries published by Martinez [9], where the relevant cases are illustrated in Figure 5.

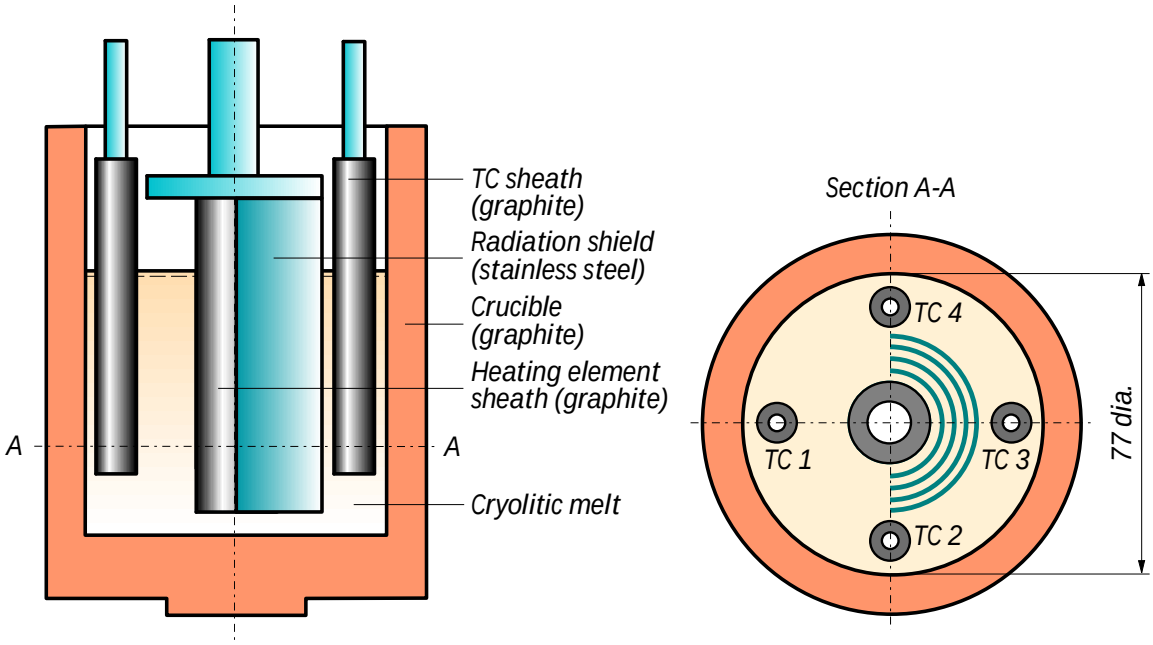

Figure 3. Experimental set-up (see the text).

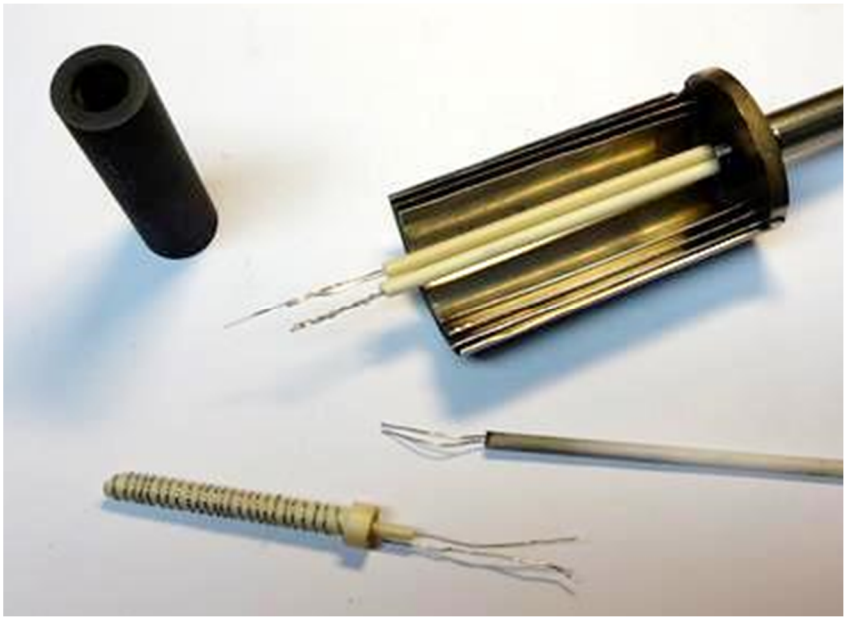

Figure 4. Equipment during assembly.

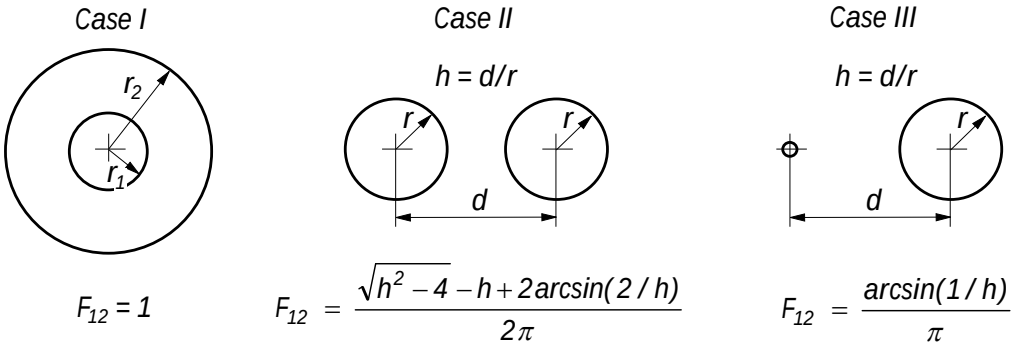

Figure 5. View factors for three cases, adapted from Martinez [9].

3.2.1. Power in the Heating Element

The relationship between the power in the heating element (P) and its temperature was estimated from an energy balance taking into account heat losses by convection and by radiation. The heat loss by natural (free) convection between the heating element and the bath was estimated from an equation by Churchill and Chu [8], where the necessary physical parameters were estimated for the bath used in the experiments (12.0 wt% excess AlF_3, 4.6 wt% CaF_2, and 3.5 wt% Al_2O_3). The radiation from the heating element to the crucible wall was calculated with F_{12} = 1 (Case I in Figure 5). The result is shown in Figure 6. As can be observed, about ¾ of the heat loss took place by convection.

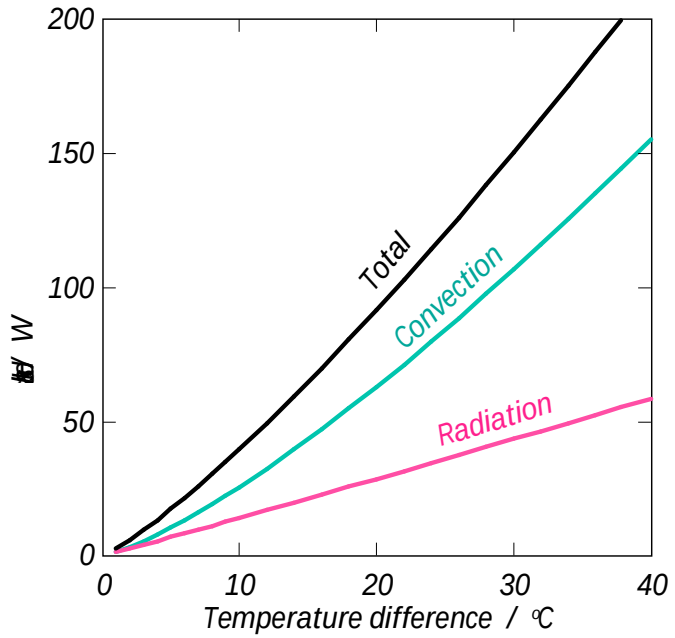

Figure 6. Heat loss from the heating element as a function of the temperature difference between the element and the bath and crucible wall.

3.2.2. Temperature Response in the Thermocouples

Radiation between the TC sheath, the crucible wall, and the heating element was also estimated using $\varepsilon_1 = \varepsilon_2 = 1$. The Churchill-Chu equation [8] was also in this case used for computing the heat loss by natural convection. Since neither Case II nor Case III in Figure 5 were directly

applicable for calculating the view factor between the heating element and the 12 mm dia. TC sheath (F_{12}), the temperature response was estimated from both cases, and it turned out that the results were similar. The view factor between the TC sheath and the crucible wall was calculated as (1-F_{12}). The resulting temperature difference between the bath/crucible wall and the TC when subjected to radiation from the heater is shown in Figure 9, together with the experimental results.

3.2.3. Radiation Shields

The effectiveness of the radiation shield was estimated using Equation (8) with F_{12} = 1 (*i.e.*, radiation shields treated as parallel surfaces without edge- or end effects). It was decided that four plates were sufficient for achieving adequate shielding. With 980 °C in the bath and at the crucible wall and 1000 °C at the heating element, the temperature at the utmost plate was estimated to be maximum 984.1 °C.

3.2.4. CFD Calculations

Since the radiation shield shown in Figure 3 is partly above the melt surface, it could be suspected that the flow by natural convection might change upon rotation of the shield, and that this could influence the recorded temperature. Therefore, CFD calculations were made (ANSYS FLUENT). It turned out, however, that there was no effect of convection at 100 W heating element power. The effect of radiation was found to be 1.4 °C, which is comparable with the simplified estimate (Figure 9).

The CFD model also computed a time constant (τ) for the TC response, which was found to be 43.5 s. Theoretically, for a first order process, 63 percent of the change is finished after one time constant, 86 percent after 2 τ, and 95 percent after 3 τ. Therefore, it was expected that most of the temperature changes would be finished within a couple of minutes. The calculated dynamic response is shown in Figure 7.

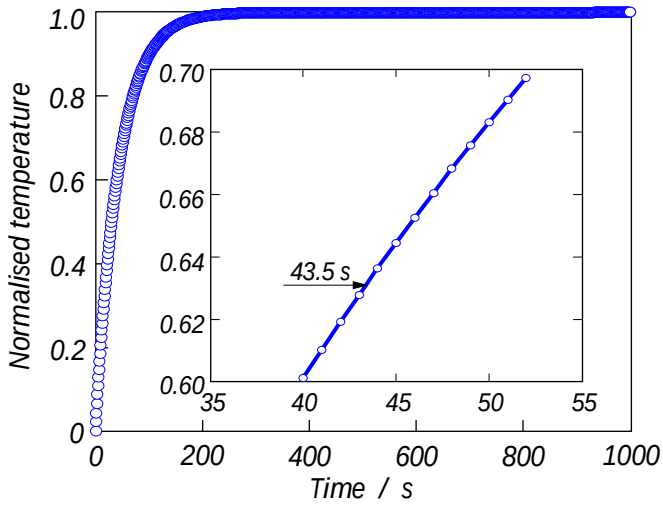

Figure 7. Calculated TC response after rotating the radiation shield.

4. Results

Two successful experimental runs were performed. The heating element turned out to be the weakest point of the set-up, and the first run, which was performed using different power settings in the heating element, was interrupted several times due to short-circuiting. Since the

bath temperature changed every time the power was adjusted, the second experiment was conducted using only one power setting (100 W) to obtain constant bath temperature. In this experiment the radiation shield was adjusted so that two and two TCs were exposed to or shielded against radiation at the same time.

Some recorded temperature courses are shown in Figure 8. Using the Figure 8 c) as an example, it can be observed that the temperature in TC 3 dropped and the temperature in TC 1 increased when the radiation shield was turned so that TC 1 became exposed to and TC 3 shielded against radiation. The responses in TCs 2 and 4 were small (half shielded and half exposed in both shield positions).

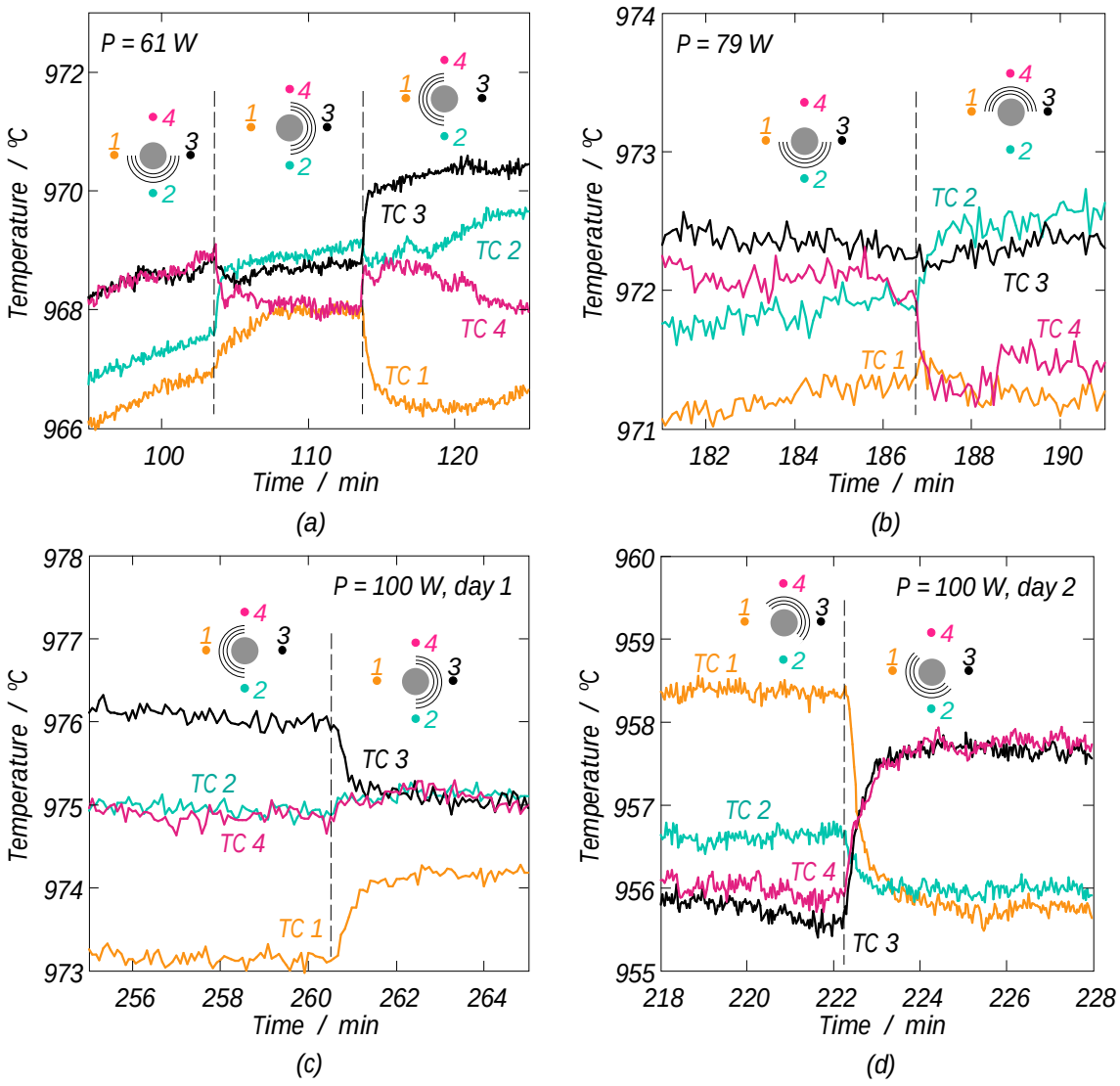

Figure 8. Some recorded temperature time *vs*. temperature curves. The position of the radiation shield is indicated in the figure.

The temperature response was not exactly the same for all thermocouples. This was particularly pronounced in the second experimental run (Figure 8 d), where TC 1 consistently had the largest temperature response and TC 2 had the smallest. The deviation was probably due to unsatisfactory fixture of the thermocouples, leading to different distances from the heating

element and, thereby, different view factors (the set-up was partly improvised, based on parts already existing in the laboratory).

A comparison between the estimated temperature changes and the experimental data is shown in Figure 9. As can be observed, experiments and estimates generally agreed well. There was also good agreement between the estimated time constant in Section 3.2.4. and the dynamic temperature behaviour after changing the position of the radiation shield.

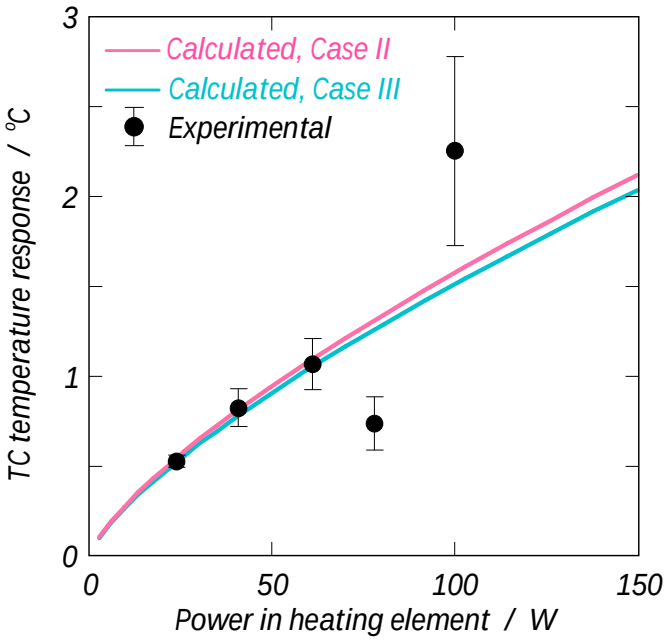

Figure 9. Temperature response as a function of the power in the heating element. Estimated values (Section 3.2.2.) and experimental data (average and standard deviation).

5. Discussion

It should be emphasized that the calculations described above were not intended to be very accurate. Also, the experimental set-up was not designed with particularly high accuracy in mind. Therefore; at the current stage, we regard that the precision is too low for allowing estimates of emissivities or attenuation coefficients, *e.g.*, by comparison between modelling and experiment. Still, the data presented above are strong indications that the heat transfer coefficient at the sideledge is influenced by radiation.

The data indicate that heat radiation can penetrate through at least 15 - 20 mm of bath without being much attenuated. Since most of (or all) bath components are transparent to radiation (Table 1), the attenuation coefficient cannot be expected to vary much with the bath composition. Dissolved metal represents one uncertainty however, since its presence makes the melt opaque, and the effect of solid particles (carbon dust) cannot be readily predicted either.

As illustrated in Figure 2, the radiation at the sideledge may represent a contribution of up to 400 $Wm^{-2}K^{-1}$ to the heat transfer coefficient. As was found in one electrolysis plant, increasing the heat transfer coefficient by that amount gave much better prediction of the superheat [5].

6. Acknowledgement

The present work was supported by the project "Superior Technology for Energy Efficient Aluminium Production" (STEP), financed by Hydro Aluminium and the Research Council of Norway. Permission to publish the results is gratefully acknowledged.

7. References

1. K.J. Fraser, M.P. Taylor, and A.M. Jenkin, Bath Heat Transfer and Mass Transport Processes in H-H Cells, *Light Metals* 1990, 221-226.
2. Y.R. Gan and J. Thonstad, Heat Transfer between Molten and Solid Cryolite Bath, *Light Metals* 1990, 421-427.
3. V.A. Khoklov, E.A. Filatov, A. Solheim, and J. Thonstad, Thermal Conductivity in Cryolitic Melts - New Data and Its Influence on Heat Transfer in Aluminium Cells, *Light Metals* 1998, 501-506.
4. A. Solheim, Some Aspects of Heat Transfer in Aluminium Reduction Cells, *Light Metals* 2011, 381-386.
5. Personal communication (2015), personnel at Primary Metal Technology, Hydro Aluminium.
6. Merck Evaporation Materials Product Catalog 2014, 8-9, http://cc-special.merck.de/pm/Evaporation_Materials_Product_Catalog/index.html#p=1
7. R.B. Bird, W.E. Stewart, and E.N. Lightfoot, *Transport Phenomena*, John Wiley & Sons, Inc., 1960.
8. S.W. Churchill and H.H.S. Chu, Correlating Equations for Laminar and Turbulent Free Convection from a Vertical Plate, *Int. J. of Heat and Mass Transfer* **18**(11), 1323-1329 (1975).
9. I. Martinez, Radiation View Factors, http://webserver.dmt.upm.es/~isidoro/tc3/Radiation%20View%20factors.pdf